


Article

On the Relationship between Thermomechanical Processing Parameters and Recrystallization Texture in AA1100 Aluminum Alloy

Hsin-Lun Yang¹, Shih-Chieh Hsiao¹, Chih-I Chang², Tien-Yu Tseng², Po-Jen Chen¹ and Jui-Chao Kuo^{1,*} 

¹ Department of Materials Science and Engineering, National Cheng-Kung University, No. 1, University Road, Tainan 70101, Taiwan; n56121107@gs.ncku.edu.tw (P.-J.C.)

² Department of New Materials Research and Development, China Steel Corporation, No. 1, Chung-Kang Road, Hsiao-Kang, Kaohsiung 81233, Taiwan; 134296@mail.csc.com.tw (T.-Y.T.)

* Correspondence: jckuo@mail.ncku.edu.tw

Abstract: In this study, 48 hot-rolling processing conditions were designed to investigate the influences of thermomechanical processing parameters on the recrystallization behavior and texture development. The hot-rolling experiments were conducted using the thermomechanical simulator Gleeble 3800 at temperatures of 275, 300, and 350 °C with strain rates of 5 and 90 s⁻¹ up to 60 and 85% reduction. The microstructure and texture analysis were measured by using the EBSD technique on a large area. Experimental results show that the Cube component maintains a volume fraction between 10% and 20%, below the 40% recrystallization fraction, but the volume fraction of Cube significantly increases between 20% and 50% above the 40% recrystallization fraction. However, the fractions of Rotated Cube (RC) and Goss components remain below 10%.

Keywords: EBSD; thermomechanical processing; recrystallization; texture; aluminum; hot rolling



Citation: Yang, H.-L.; Hsiao, S.-C.; Chang, C.-I.; Tseng, T.-Y.; Chen, P.-J.; Kuo, J.-C. On the Relationship between Thermomechanical Processing Parameters and Recrystallization Texture in AA1100 Aluminum Alloy. *Metals* **2024**, *14*, 962. <https://doi.org/10.3390/met14090962>

Received: 28 July 2024

Revised: 18 August 2024

Accepted: 23 August 2024

Published: 25 August 2024



Copyright: © 2024 by the authors. Licensee MDPI, Basel, Switzerland. This article is an open access article distributed under the terms and conditions of the Creative Commons Attribution (CC BY) license (<https://creativecommons.org/licenses/by/4.0/>).

1. Introduction

The hot-rolling texture of aluminum alloys without dynamic recrystallization is significantly different from their cold-rolling texture. The texture of hot-rolled commercial purity aluminum typically contains the Cube component and the β -fiber rolling orientations of brass (B), copper (C), and S. The dominant texture in recrystallized grains is the Cube component, whereas the β -fiber rolling orientations are dominant in deformed grains [1]. Hollinshead and Sheppard [2] reported that the B component appears at appreciable strengths at low reductions and increases with the reduction for AA 3004 aluminum alloy. Bate and Oscarsson [3] reported for hot-rolled Al–1% Mn–1.2% Mg alloy that C, S, and B have roughly similar densities, with the maximum near copper at a strain of 2, while S and B doubled in intensity, and copper decreased slightly at a strain of 5. Furthermore, the observation that a strong β fiber rolling texture forms during hot deformation is consistent with the experimental observations of Daaland et al. [4], Engler et al. [5], Panchanadeeswaran and Field [6], Vatne et al. [7], Maurice and Driver [8], Duckham et al. [9], and Bate et al. [10].

Bacroix et al. [11] reported for AA 1200 and AA 8979 alloys that the texture strength increases with temperature, and a significant increase in the B component occurs without a complete orthotropic symmetry with the increasing temperature. Samajdar et al. [12] reported that the volume fractions of the C and S components decrease with the increase in temperature or decrease in strain rate. Duckham et al. [9] attributed this strong β fiber rolling texture to the healing of the dislocations within the subgrains and the consumption of subgrains with scattered orientations during the dynamic recovery, which is generally enhanced at high deformation temperatures. Aryshenskii et al. [13] found that increasing the alloying component of magnesium resulted in an increase in Brass and a decrease in S and Copper during hot deformation of aluminum alloys.

The increase in the B component is attributed to the increase in the strain rate sensitivity index by Engler et al. [5], the additional activation of other non-octahedral slip systems at very high deformation temperatures by Le Hazif et al. [14], Le Hazif et al. [15], Maurice and Driver [8], and Bacroix and Jonas [16], and the differential dynamic grain growth by Bate et al. [10]. Bacroix and Jonas [16,17] applied full constraint (FC) and relaxed constraint (RC) models, considering cross-slip systems, to predict the hot-rolling texture. The concurrent activation of both slip and cross-slip systems leads to the presence of three main rolling components, namely, the C, S, and B orientations, in proportions that vary with the CRSS ratios of the different systems. In rolling, the activation of the {100}(110) systems leads to the prediction of a strong S component, whereas the slip on the {110} planes mainly produces a C component, and that on the {112} planes produces a B-type texture. Hirsch and Luecke [18] also used Taylor-type theories under full and relaxed constraints and found that the exact {011}<211> B orientation is found for a Sachs-type RC model in which the grain TD/RD shear is completely relaxed. However, non-octahedral slip has been observed at low strain rates $< 10^{-3} \text{ s}^{-1}$ but not yet at high strain rates $> 10 \text{ s}^{-1}$, which is typical of industrial hot-rolling schedules. Sachs-type grain relaxation generally leads to unreasonably high strain rate incompatibilities between grains.

After discussing the increasing B component, we now discuss the recrystallized Cube component during hot rolling. Hollinshead and Sheppard [2] reported that the Cube component forms in small quantities during interpass reheat recrystallization for AA 3004 aluminum alloy. Maurice et al. [19] reported that the rotation of the {112}(111) C component is predicted toward the {110}(112) B and {123}(634) S components at high rate sensitivity and TD/RD shear values. Vatne et al. [7] reported that the recrystallized Cube component is enhanced by a high initial Cube fraction in many Cube bands, a low Zener–Hollomon parameter, and a high strain. Liu and Morris [20] reported for AA 5052 aluminum alloy that the initial orientations at elevated temperatures are more easily rotated to the β fiber between the B and S orientations than to the C orientation, whereas those at room temperature are more easily rotated to the S orientation than to the B and C orientations. Alvi et al. [21] reported that Cube recrystallized grains have a strong nucleation advantage at all annealing temperatures, while a growth rate advantage is observed for Cube recrystallized grains at low annealing temperatures. In addition, Cube-recrystallized grains preferentially grow into deformed S grains but grow most slowly into deformed B grains. Wang et al. [22] reported that the cold-rolled texture of Copper and S components is consumed and transformed into the Cube component after annealing.

Vatne et al. [7], Samajdar et al. [12], and Bate et al. [23] studied the stability of the Cube orientation during the hot deformation of aluminum alloys. Vatne et al. [7], Duckham et al. [9], and Bate et al. [23] reported that the stability of the Cube orientation increases with the decreasing Z value. Maurice and Driver [24] attributed the enhanced stability of the Cube orientation during hot deformation to the activation of non-octahedral slip systems. Gatti and Bhattacharjee [25] reported that homogenous recovery eliminates the nucleation advantage of the Cube regions originating from the preferentially recovered structure and significantly weakens the Cube component.

Although numerous experimental studies have been carried out in the past decades on recrystallization kinetics, the experimental materials and testing conditions are different, preventing the comparison of the number of results with the other results. In this work, we designed 12 hot-rolling process conditions to understand the effects of the thermomechanical process history on the recrystallization texture control. The hot-rolling conditions were experimentally simulated by using double-hit compression experiments as the thermal–mechanical simulator.

2. Experiments

2.1. Experimental Materials and Sample Preparation

The dimensions of the annealed AA1100 aluminum alloy provided by China Steel Corporation (Kaohsiung, Taiwan) were reduced to 25 mm \times 15 mm \times 38 mm for the

hot-compression experiment. The corresponding chemical composition is shown in Table 1. The double-hit compression experiment was conducted using the thermal–mechanical simulator Gleeble 3800 (Dynamic Systems Inc., Poestenkill, USA) at temperatures of 275 °C, 300 °C, and 350 °C, with low and high strain rates of 5 s^{−1} and 90 s^{−1}, to the thickness of 6.5 mm (60% reduction) and 2.5 mm (85% reduction), respectively. The dimensions of the flat punch’s contact area are 42 mm × 10 mm. Figure 1 illustrates the geometry of the specimen after 60% reduction. After the hot compression, the specimens were isothermally annealed in a salt bath at the corresponding temperatures of 275 °C, 300 °C, and 350 °C for recrystallization. The above-mentioned processes of hot compression and annealing are illustrated in Figure 2. The thermomechanical processing parameters (TMPs), including temperature, strain rate, and reduction ratio, and the annealing parameters, including temperature and time, are listed in Table 2. A total of 48 specimens were prepared to systematically investigate the influence of thermomechanical processing parameters on the recrystallization behavior.

Table 1. Chemical composition of AA1100 aluminum alloy (wt%).

Alloy	Si	Fe	Cu	Mn	Mg	Cr	Ti	Al
AA1100	0.17	0.38	0.09	0.004	0.002	0.001	0.03	Balance

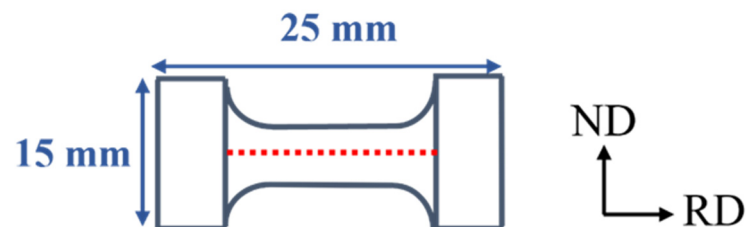


Figure 1. Schematic cross-section view of the specimen and the cross-section dimensions of the measured specimens for double-hit compression experiment under compression along the ND direction, where the measured area is at the middle cross-section in the red dotted line (called $s = 0$), and the thickness is 6.5 mm for 60% reduction and 2.5 mm for 85%.

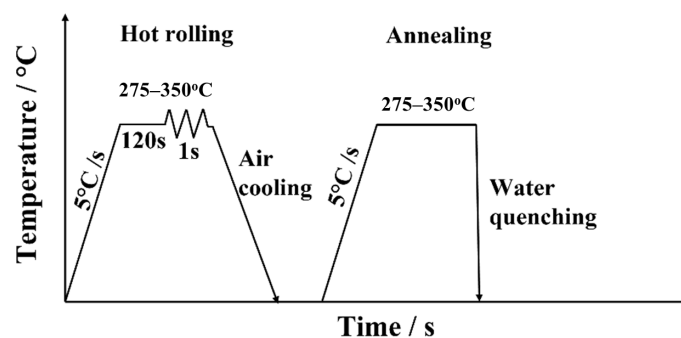


Figure 2. Schematic of thermo-mechanical processes, including hot rolling and annealing process for double-hit compression experiment in Gleeble®.

After thermomechanical processing, the middle area of the ND-RD section with a 10 mm width was first cut from all H-shaped test specimens, as shown in Figure 1, using the low-speed precision cutter Plusover S150 (Yu-Chang Instruments Co., Kaohsiung, Taiwan). Then, the cut specimens were rotated 90 degrees, and the cut middle area of the ND-TD section with a 10 mm width cut to obtain the 10.0 mm × 10.0 mm sample. In the end, the specimens were ground to the middle surfaces at $s = 0$. Later, the specimens were ground using #1500, #2500, and #4000 and cleaned with ethanol. Subsequently, the specimens were polished using silica suspensions with particle sizes of 3, 1, and 0.25 μm . Finally, electropolishing was performed using a perchloric acid solution and ethanol at 30 V and $-15\text{ }^\circ\text{C}$.

Table 2. Thermomechanical processing parameters (TMPs) of temperature (T), strain rate ($\dot{\epsilon}$), and reduction ratio (ϵ) tested on a Gleeble thermomechanical simulator and annealing time (t) of AA1100 alloy.

Name	T ($^{\circ}\text{C}$)	TMPs		Annealing Time t (s)				
		$\dot{\epsilon}$ (s^{-1})	ϵ (%)					
T275-1 (1)	275	5	60	0	1800	4800	10,800	28,800
T275-2 (2)		5	85					
T275-3 (3)		90	60					
T275-4 (4)		90	85					
T300-1 (5)	300	5	60	0	300	900	3000	9000
T300-2 (6)		5	85					
T300-3 (7)		90	60					
T300-4 (8)		90	85					
T350-1 (9)	350	5	60	0	30	150	300	900
T350-2 (10)		5	85					
T350-3 (11)		90	60					
T350-4 (12)		90	85					

2.2. EBSD Measurements

After the sample preparation, the EBSD measurements taken using Hitachi SU5000 (Hitachi High-Tech Corporation, Tokyo, Japan) with EDAX VELOCITY PLUS (AMETEK EDAX, LLC, Mahwah, USA) were used to examine the microstructure and texture of the AA1100 aluminum alloy on the surface parallel to the normal direction (ND), as shown in Figure 1, at an accelerating voltage of 20 kV under the tilt angle of 70° , where the measured area was $2.0 \text{ mm} \times 1.6 \text{ mm}$, with a step size of $1.0 \mu\text{m}$. Here, the microstructure and the texture were analyzed using the OIM Analysis 8.5 software (version 8.5, AMETEK EDAX, LLC, Mahwah, USA), and the volume fraction of the components was calculated using the LaboTex 3.0 software. The volume fraction of the major components shown in Table 3 was calculated by integrating the orientation intensity of $f(g)$ within a Euler space with $\Delta\varphi_1 = \Delta\Phi = \Delta\varphi_2 = 10^{\circ}$.

Table 3. Miller index of texture components in hot-rolled aluminum alloy.

Texture Component	Miller Index
C	{112}<111>
S	{123}<634>
B	{110}<112>
Cube	{001}<100>
$\text{RC}_{20^{\circ}\text{RD}}$	{013}<001>
Goss	{110}<001>

3. Results and Discussion

3.1. Effects of Thermomechanical Processing Conditions on Recrystallization

We measured 3,200,000 points over a large area with $2.0 \text{ mm} \times 1.6 \text{ mm}$ with a scanning step of $1 \mu\text{m}$ for each specimen in order to collect a large dataset to calculate the orientation distribution function, which shows the same distribution by calculation from X-ray pole figures. The magnified inverse pole figure maps of all the hot-rolled microstructures are shown in Figures 3 and 4 after the thermomechanical processing conditions of the hot rolling, as shown in Table 2, without further annealing, which is called the hot-rolled state. However, there are some black points in Figures 3 and 4, which belong to non-indexed points due to heavily deformed structures or dislocation structures. After recrystallization, recrystallized microstructures are revealed in Figures 5 and 6, while some black points are found in Figures 5a,e and 6b,d due to partial recrystallization.

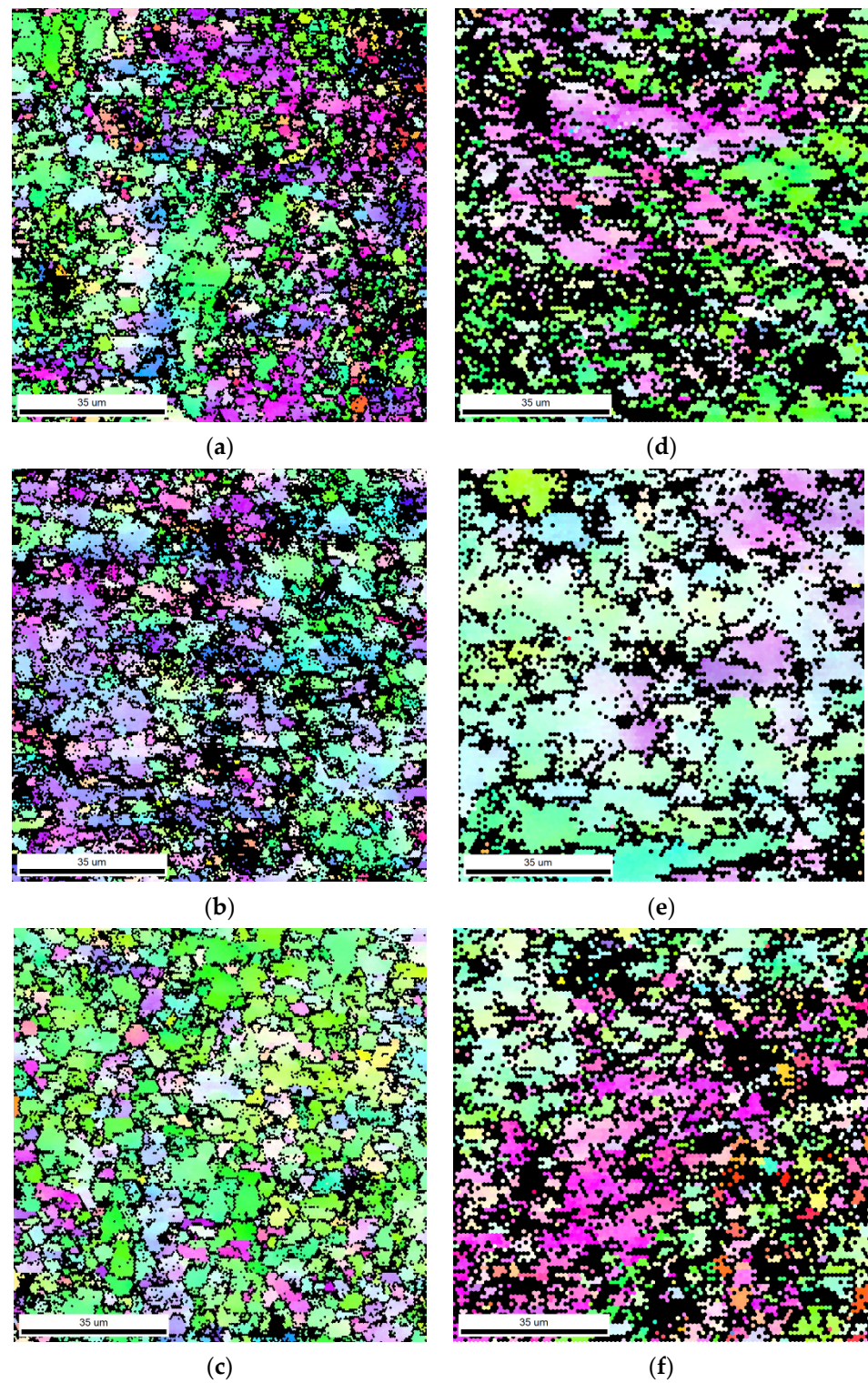


Figure 3. Magnified inverse pole figure (IPF) map of hot-rolled microstructure of AA1100 alloy at (a,d) 275 °C, (b,e) 300 °C, and (c,f) 350 °C with strain rates of (a–c) 5 s^{-1} and (d–f) 90 s^{-1} for 60% strain.

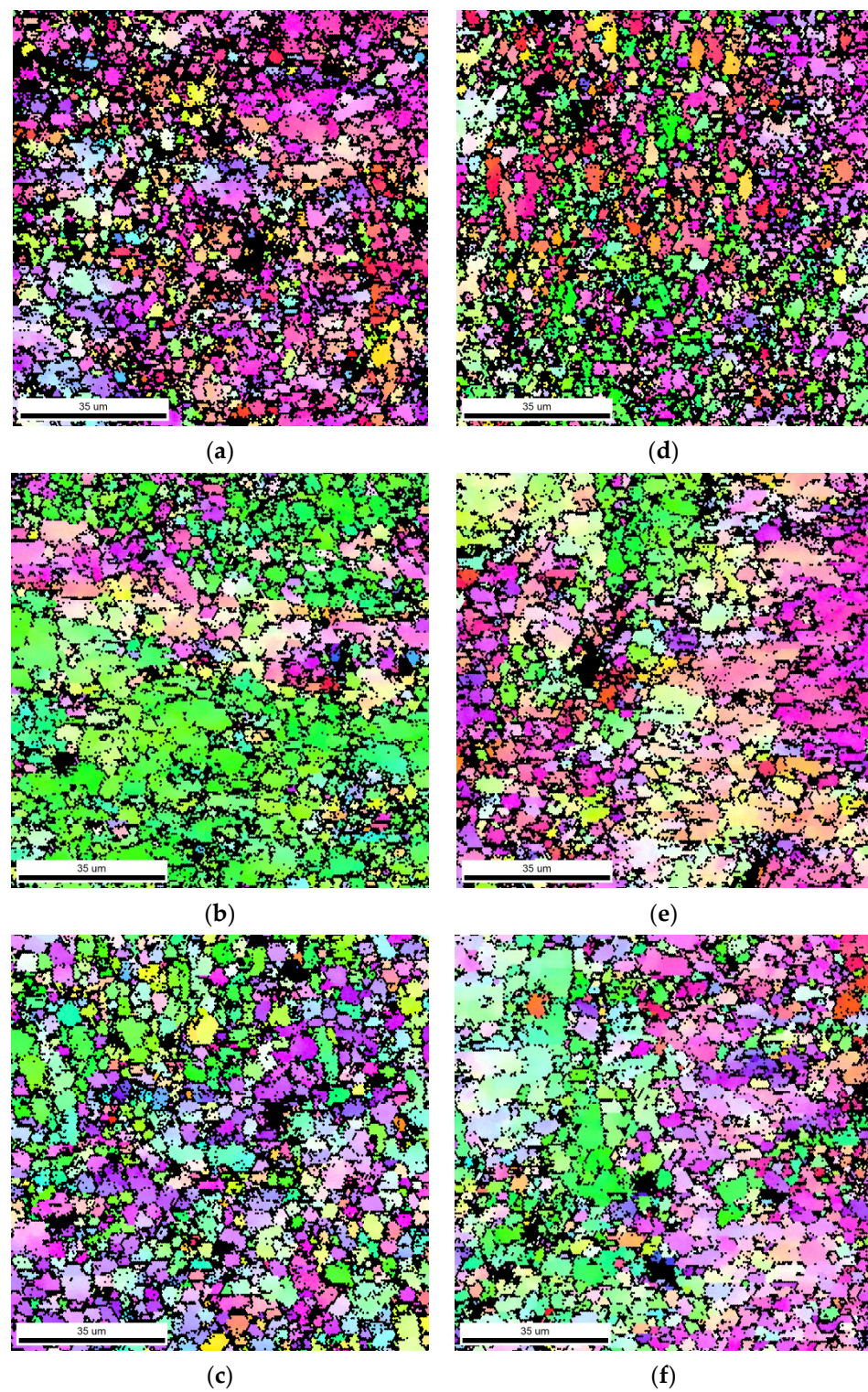


Figure 4. Magnified inverse pole figure (IPF) map of hot-rolled microstructure of hot-rolled AA1100 alloy at (a,d) 275 °C, (b,e) 300 °C, and (c,f) 350 °C with strain rates of (a–c) 5 s^{-1} and (d–f) 90 s^{-1} for 90% strain.

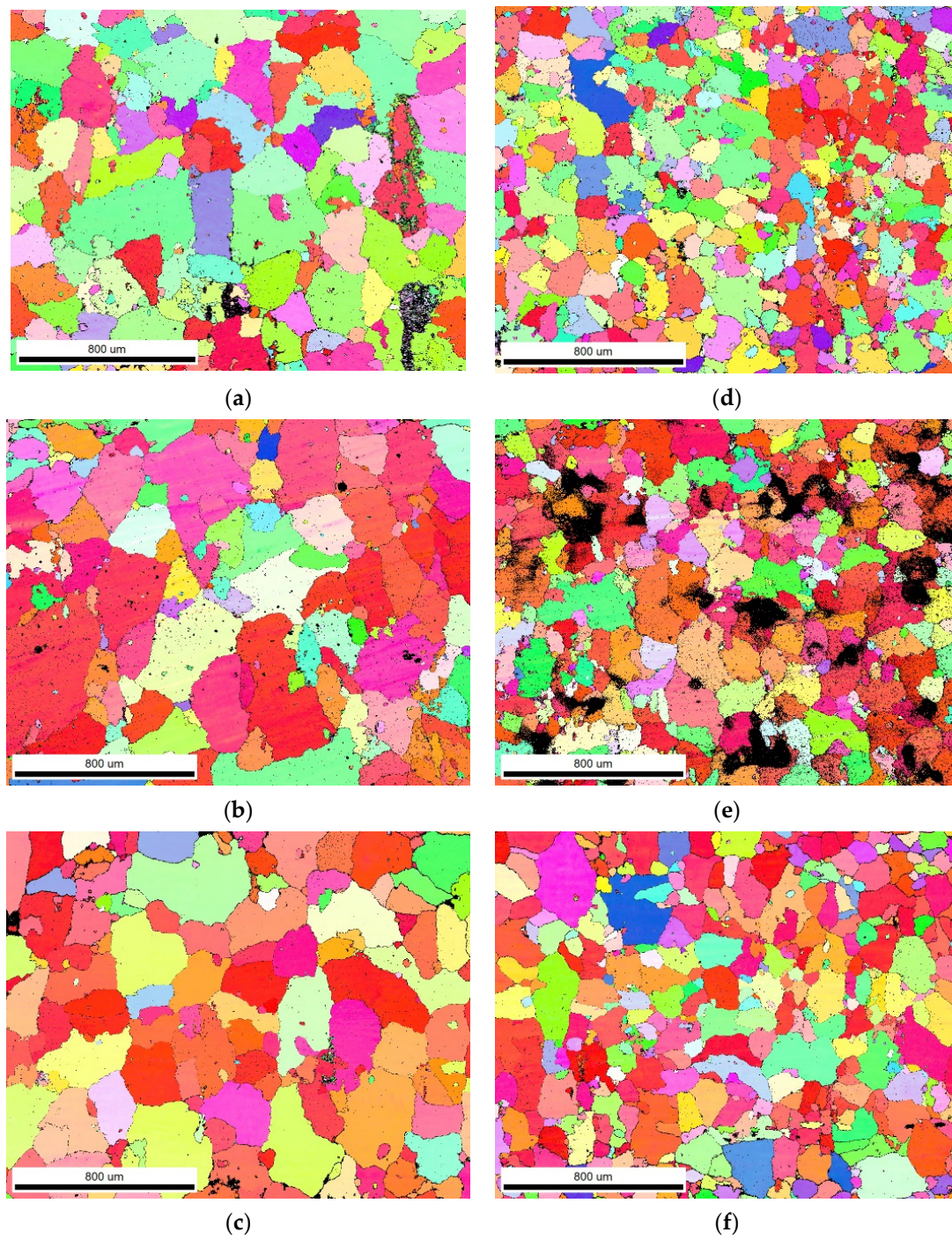


Figure 5. Magnified inverse pole figure (IPF) map of recrystallized microstructure of AA1100 alloy at (a,d) 275 °C, (b,e) 300 °C, and (c,f) 350 °C with strain rates of (a–c) 5 s^{-1} and (d–f) 90 s^{-1} for 60% strain.

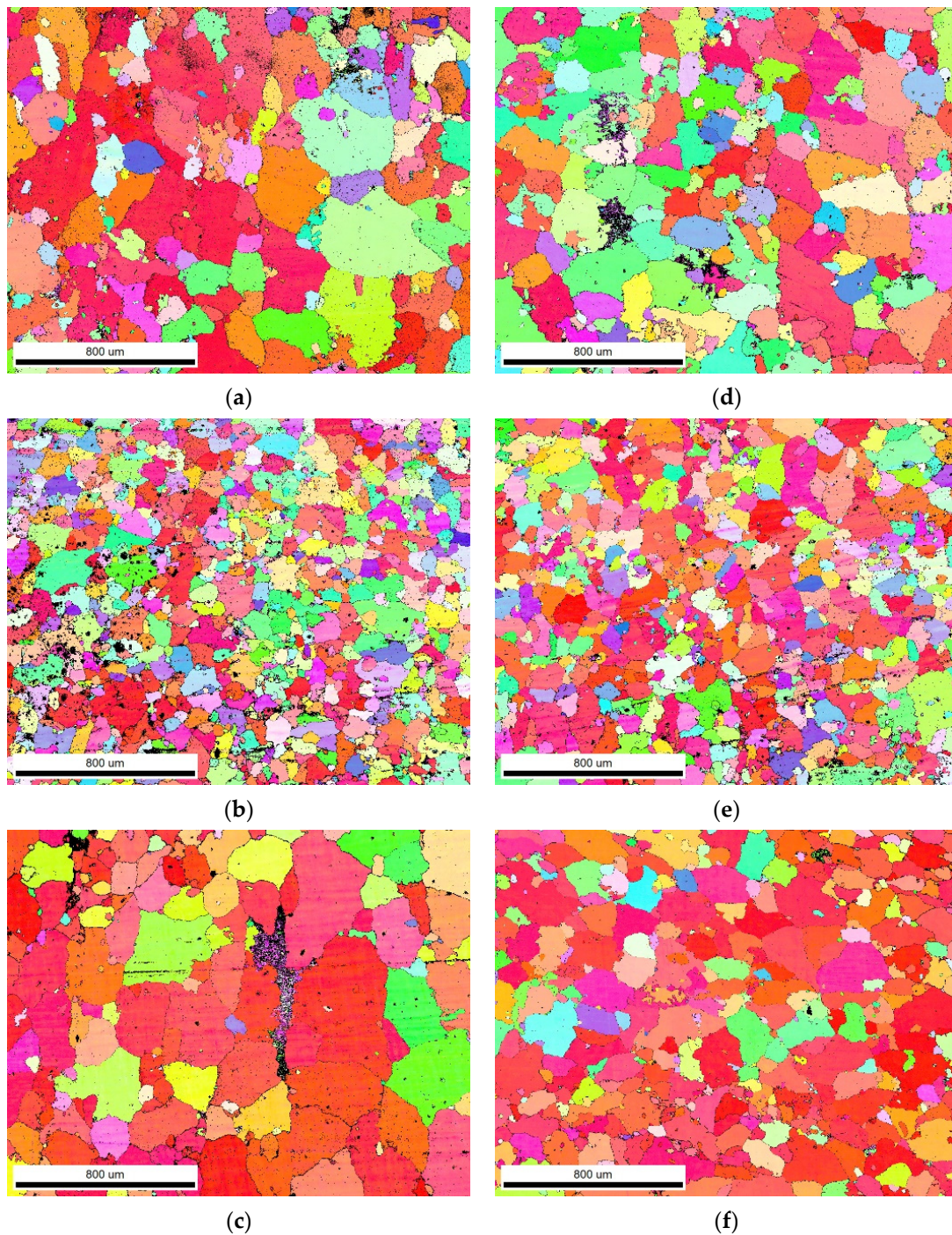


Figure 6. Magnified inverse pole figure (IPF) map of recrystallized microstructure of hot-rolled AA1100 alloy at (a,d) 275 °C, (b,e) 300 °C, and (c,f) 350 °C with strain rates of (a–c) 5 s^{-1} and (d–f) 90 s^{-1} for 90% strain.

The kernel average misorientation (KAM) calculated within approximately the seventh nearest neighbor was utilized to distinguish between recrystallization and deformation in terms of the KAM value. The simultaneous Gaussian fitting using two peaks was applied on the KAM distribution curve to separate two peaks between low and high KAM values, as shown in Figure 7d. The intersection of the two curves was defined as the threshold of 1.58° in Figure 7d between recrystallization and deformation. The value of KAM can be considered the index of dislocation density. Thus, the KAM value of deformation shows a high value in Figure 7b, and that of recrystallization indicates a low value due to a low

dislocation density in Figure 7c. In addition, the recrystallization fraction was estimated by the integration of the area fraction within the range of KAM from zero to the threshold of 1.58° . Here, we took the condition of 85% hot-rolled AA1100 alloy at 350°C , for instance, to demonstrate the determination procedure of the threshold value of KAM. The threshold value of KAM lies in the range between 1.23 and 1.5, and the mean value is 1.33 for the 12 conditions. The results of the different values reveal the reproducibility question, and thus, it is necessary to keep improving this technique.

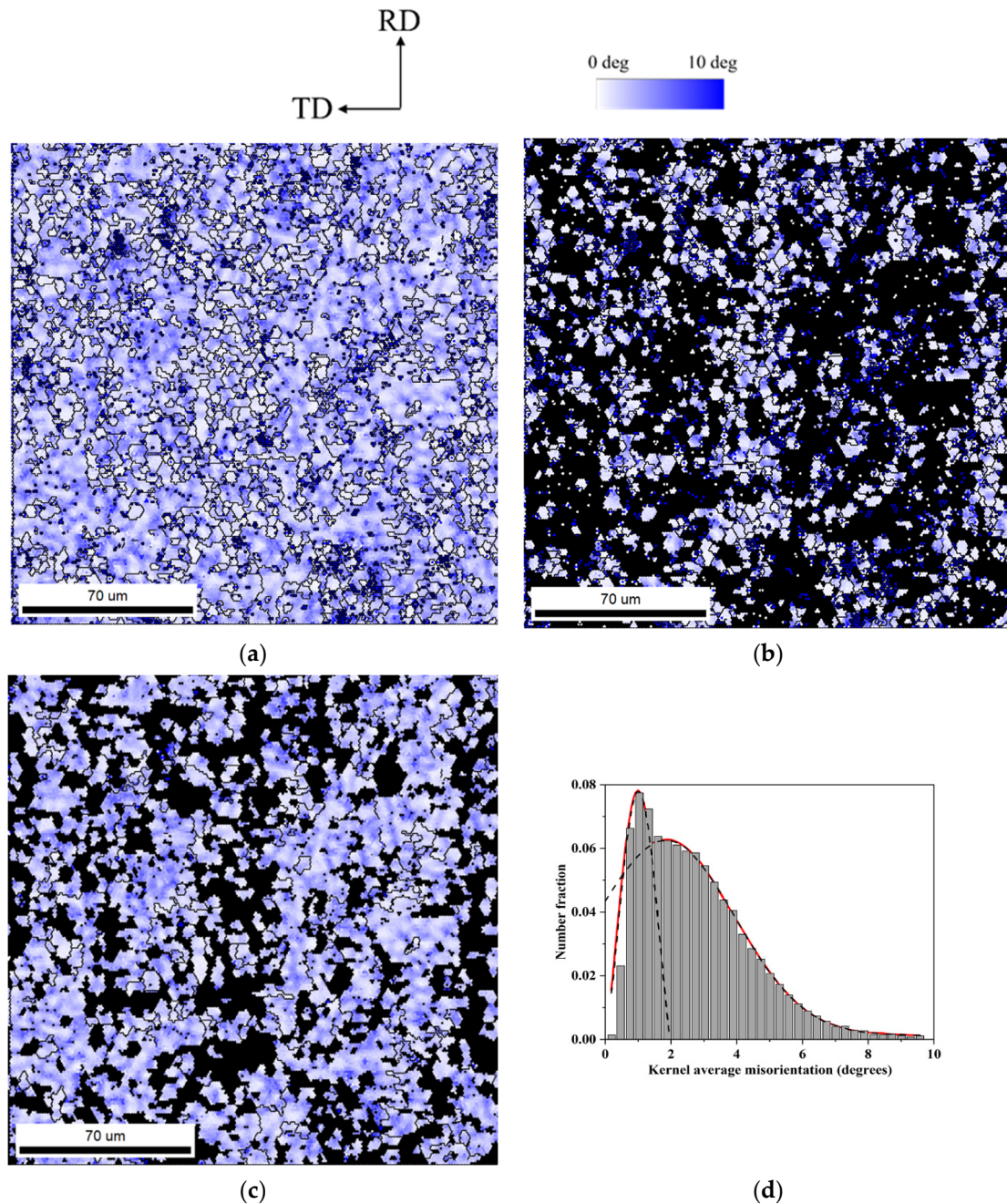


Figure 7. (a) KAM map, (b) KAM map with $\text{KAM} \leq 1.58^\circ$, and (c) KAM map with $\text{KAM} > 1.58^\circ$, (d) KAM histogram of 85% hot-rolled AA1100 alloy at 350°C . The red line represents the simultaneous Gaussian fitting curve, which is composed of two separate peaks indicated by the dashed lines with an intersection point at 1.58.

The recrystallization behavior is illustrated in Figure 8, where the recrystallization fraction determined by the above-mentioned KAM method is plotted with respect to the

annealing time at annealing temperatures of 275 °C, 300 °C, and 350 °C after the double-hit compression in the AA1100 alloy. Except at 300 °C, the typical recrystallization curve is a sigmoidal curve with an S shape at 275 °C and 350 °C. Furthermore, it is observed that the fitting curves do not fit the data well in Figure 8a, especially for the condition of 5 and 60% at 275, 300, and 350 °C, which means a low strain rate and a low reduction ratio.

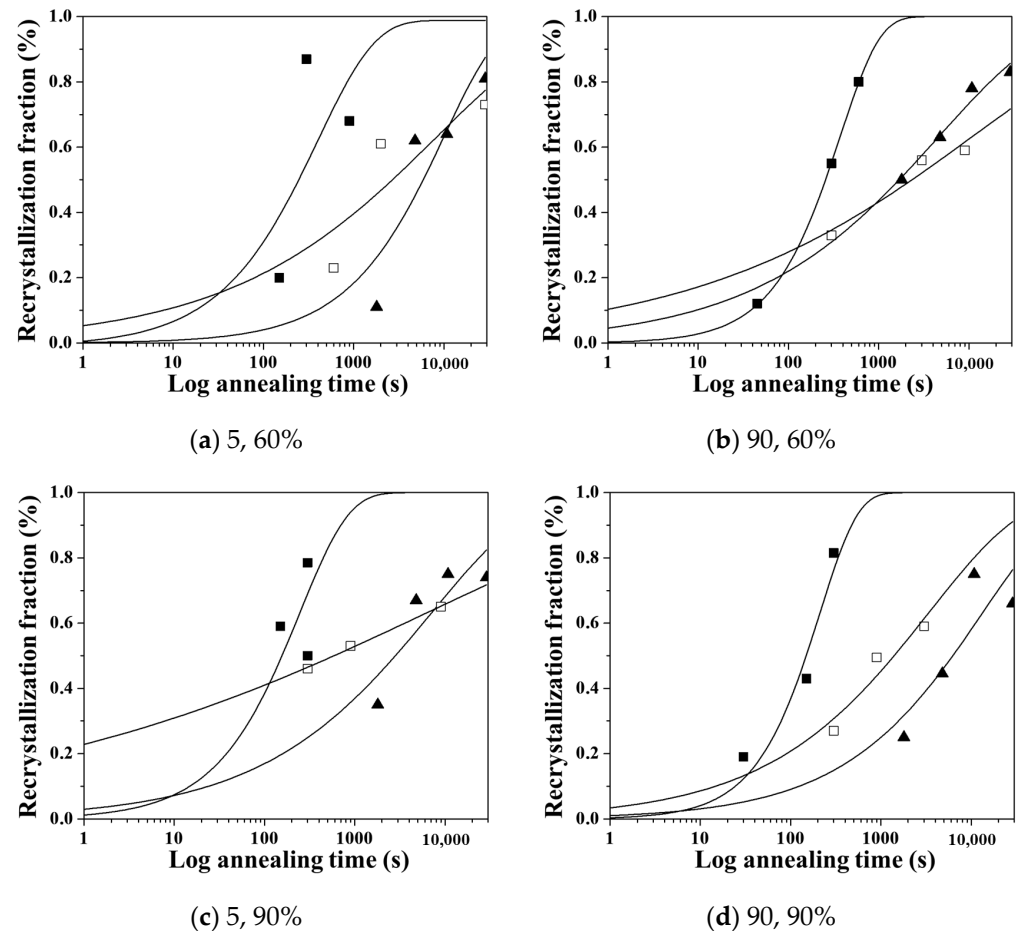


Figure 8. Recrystallization fraction as a function of annealing time at strain rates of (a,c) 5 s⁻¹ and (b,d) 90 s⁻¹ after (a,b) 60% and (c,d) 90% in hot-rolled AA1100 alloy (▲: 275 °C, □: 300 °C, ■: 350 °C).

The Johnson–Mehl–Avrami–Kolmogorov (JMAK) equation is usually used to describe the recrystallization fraction as a function of time as follows [26]:

$$X_v = 1 - \exp\left(-0.693\left(\frac{t}{t_{0.5}}\right)^{n_R}\right), \quad (1)$$

where X_v is the recrystallized fraction, $t_{0.5}$ is the time required for the recrystallization fraction of 50%, t is the time, and n_R is the JMAK exponent. The fitting parameters are shown in Table 4. The n_R value of the recrystallization exponent lies in the range between 0.15 and 1.03 in Table 4. It is noted that the recrystallization fraction X_0 at the beginning is larger than 0 at the seven conditions in Table 4, where the recrystallization fraction X_0 is predicted by using the fitting curve at $t = 0$. This finding indicates that different thermomechanical processing conditions possibly lead to the partial recrystallization during the thermomechanical processing. Therefore, this partial recrystallization during the thermomechanical processing reduces the driving forces for the following recrystallization, and the n_R value of the recrystallization exponent decreases.

Table 4. Fitting parameters of n_R -value, $t_{0.5}$, and the volume fraction of recrystallization at the beginning X_0 for different thermo-mechanical processing conditions of reduction ratio (ϵ), strain rate ($\dot{\epsilon}$), and temperature (T) in AA1100 alloy.

T (°C)	$\dot{\epsilon}$ (s ⁻¹)	ϵ (%)	Z (s ⁻¹)	n_R	$t_{0.5}$ (s)	X_0 (%)
275	5	60	5.75×10^{15}	0.69	5894	0
		85		0.39	2806	0.03
	90	60	1.04×10^{17}	0.36	1685	0.05
		85		0.48	6238	0.01
300	5	60	1.27×10^{15}	0.32	2683	0.05
		85		0.15	584	0.22
	90	60	2.28×10^{16}	0.23	2336	0.10
		85		0.41	1395	0.04
350	5	60	8.85×10^{13}	0.68	500	0
		85		0.80	108	0
	90	60	1.59×10^{15}	0.98	136	0
		85		1.03	169	0

Meanwhile, the $t_{0.5}$ value is usually expressed in terms of Z and annealing temperature T on $t_{0.5}$ as follows [27]:

$$t_{0.5} = A\epsilon^{-a}Z^{-b}\exp\left(\frac{Q}{RT}\right), \quad (2)$$

where a is 1.5, b is 0.75, Q is 220 kJ mol⁻¹, and k is 1.5×10^{-4} . Thus, according to Equation (2), $t_{0.5}$ decreases as Z increases at a constant annealing temperature, as shown in Table 4. This shows a decrease in $t_{0.5}$ as T increases at constant Z and strain. According to Sellars and McTegart [28], the hot working conditions of the temperature and the strain rate are empirically combined in the Zener–Holloman factor as

$$Z = \dot{\epsilon} e^{Q/RT}, \quad (3)$$

where $\dot{\epsilon}$ is the strain rate, Q is the deformation activation energy, R refers to the ideal gas constant, and T is the deformation temperature. The deformation activation energy of Q is 156 kJ/mol, as previously reported [29]. Therefore, we can plot the n_R value of recrystallization obtained from the experiments as functions of $\log Z$ and reduction rate ϵ in the 3D diagram, where the Z values are listed in Table 4 in descending order with respect to temperature (T) and strain rate ($\dot{\epsilon}$).

It is observed in Table 4 that the value of n_R is high with Z and deformation reduction, which corresponds to low deformation temperature, high strain rate, and high reduction. By contrast, the values of n_R are small at high Z and low deformation reduction or low Z and high deformation reduction, which correspond to low deformation temperature, high strain rate, and low reduction and high deformation temperature, low strain rate, and high reduction, respectively.

3.2. The Kinetic Behavior of the Texture Components

To understand the kinetic behavior of the texture components, we also adapted the concept of the JMAK equation, and the fraction of texture component X_t at time t is expressed in terms of time as follows [30]:

$$\frac{X_t - X_i}{X_f - X_i} = 1 - \exp\left(-0.693\left(\frac{t}{t_{0.5}}\right)^{n_T}\right), \quad (4)$$

where X_i and X_f are the volume fractions of the component at the beginning and after recrystallization, respectively. In addition, we assumed that the constant of 0.693 is orientation-independent in this study. The developments of the recrystallization textures are plotted as a function of annealing time for the 12 hot-rolling processing conditions in Table 2, as shown in Figures 9 and 10. The fitting parameters of the n_T value and $t_{0.5}$ for the

C, S, B, Cube, RC, and G components are shown in Table 5 for the 12 thermo-mechanical processing conditions.

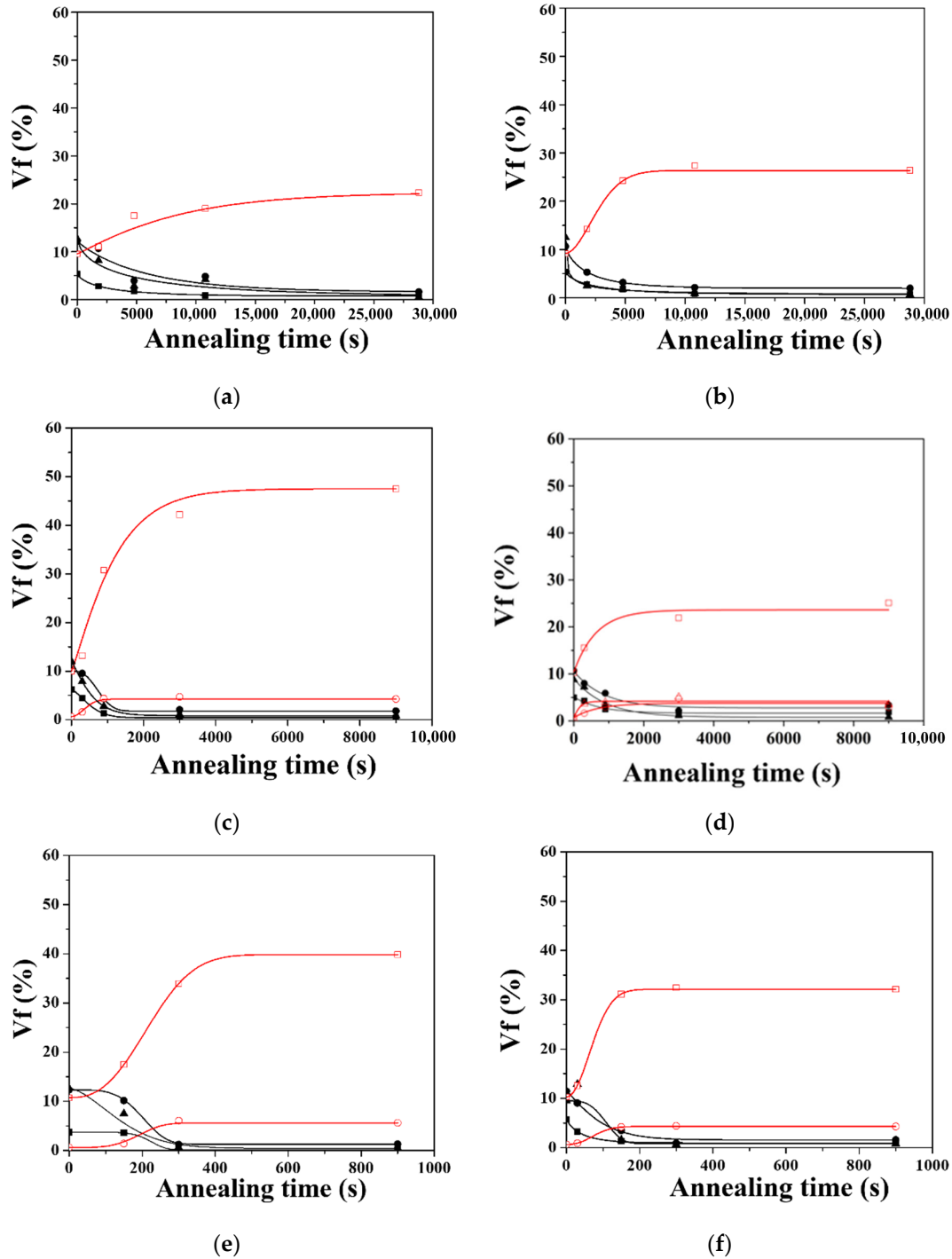


Figure 9. Volume fraction of six texture components as a function of annealing time at strain rates of (a,c,e) 5 s^{-1} and (b,d,f) 90 s^{-1} for 60% hot-rolled AA1100 alloy at (a,b) 275, (c,d) 300, and (e,f) 350 °C. (C: ■, S: ●, B: ▲, Cube: □, RC_{20RD}: ○, Goss: △).

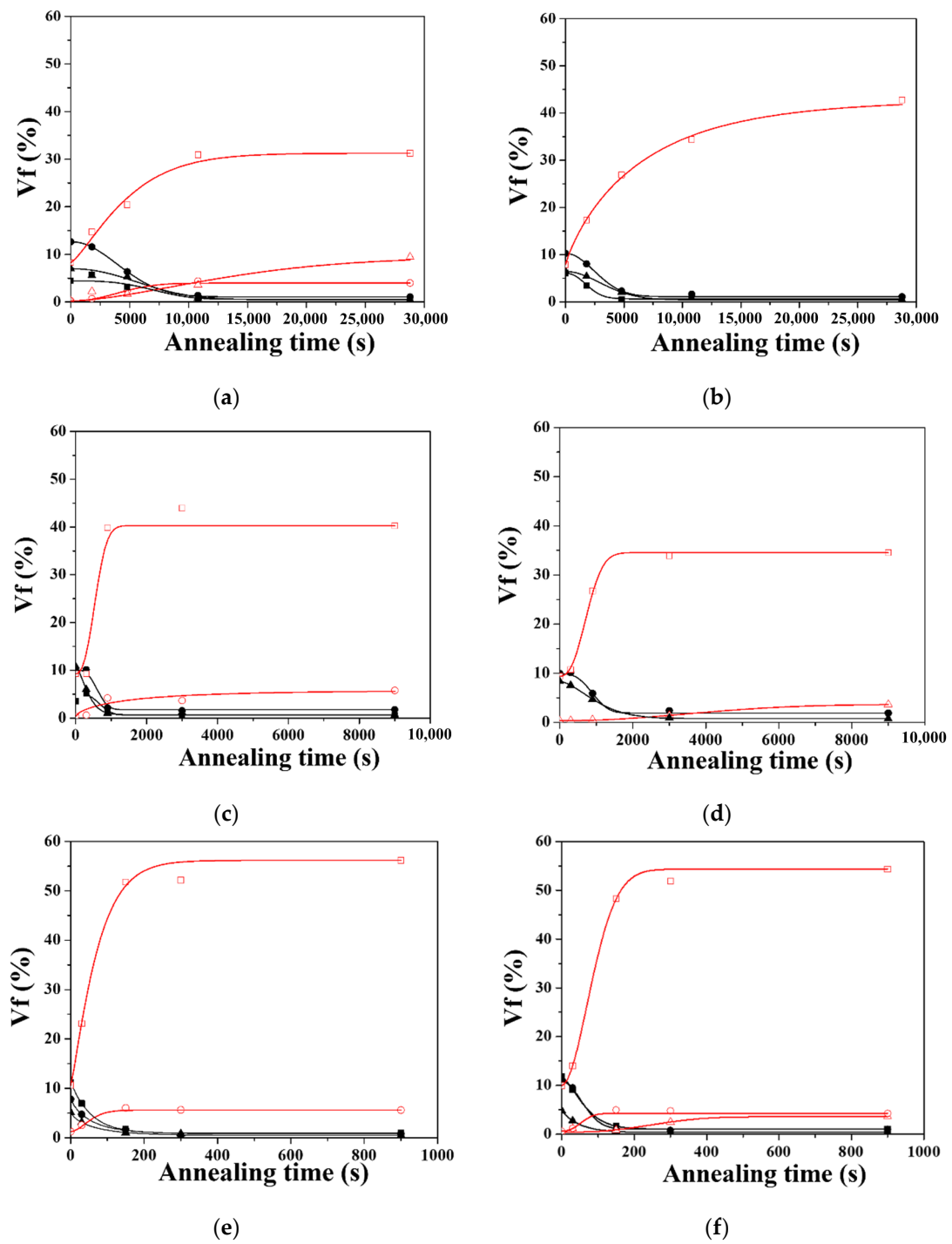


Figure 10. Volume fraction of C, S, B, Cube, RC, and G components as a function of annealing time at strain rates of (a,c,e) 5 s^{-1} and (b,d,f) 90 s^{-1} for 85% hot-rolled AA100 alloy at (a,b) 275, (c,d) 300, and (e,f) 350 °C. (C: ■, S: ●, B: ▲, Cube: □, RC_{20RD}: ○, Goss: △).

Table 5. Fitting parameters of n_T -value and $t_{0.5}$ for C, S, B, Cube (Cb), RC_{20°RD} (RC), and Goss (G) components at 12 thermo-mechanical processing conditions in AA1100 alloy.

	Name	1	2	3	4	5	6	7	8	9	10	11	12
C	n	-	2.20	0.73	3.15	1.49	3.00	1.71	-	7.01	0.80	0.85	1.00
	$t_{0.5}$ (s)	-	1919	1513	7070	458	693	541	-	221	39	28	34
S	n	0.95	2.02	0.77	2.07	2.77	3.00	1.04	3.00	4.29	1.06	1.20	1.46
	$t_{0.5}$ (s)	3910	2831	1200	4524	745	610	513	900	200	39	68	56
B	n	0.61	1.95	0.34	2.20	1.20	1.52	1.43	1.60	1.65	0.87	3.50	2.00
	$t_{0.5}$ (s)	2355	3470	107	6187	418	316	659	936	131	37	108	62
Cb	n	1.09	0.87	1.82	1.28	1.16	2.50	-	2.50	2.60	1.18	2.06	1.88
	$t_{0.5}$ (s)	6000	4348	2613	3920	890	554	-	742	218	57	72	86
RC	n	-	-	-	2.25	2.00	2.37	1.21	-	4.00	1.74	2.37	2.40
	$t_{0.5}$ (s)	-	-	-	4335	398	900	780	-	190	50	76	65
G	n	-	-	-	1.59	-	-	0.43	2.14	-	-	3.75	2.68
	$t_{0.5}$ (s)	-	-	-	12,300	-	-	101	3922	-	-	550	255

In this study, the deformation texture is composed of three main components, C, S, and B, and the recrystallization texture consists of Cube, RC, and G components. It was observed that the three deformation texture components, C, S, and B, decrease, but three recrystallization texture components, Cube, RC, and G, increase with increasing annealing time at 275, 300, and 350 °C, as shown in Figures 9 and 10. The recrystallization component of the Cube with a volume fraction larger than 30% increases significantly in comparison with the RC and G components. Furthermore, the initial volume fraction of the Cube component is larger than 10% at the beginning of recrystallization. This observation is in agreement with the occurrence of partial recrystallization during the thermomechanical processing, and the Cube is retained in the thermomechanical processing.

3.3. Relationship between Recrystallization and Texture

As discussed above, the 12 hot-rolling processing conditions reveal the different fractions of recrystallization after the hot-rolling process. During the hot-rolling process, we take the retained recrystallization fraction into account, which is called the initial fraction for the following annealing process. In addition, we separate the deformation and recrystallization textures in order to understand the competition between both textures during the annealing process. The texture components of C, S, and B belong to the deformation texture, and the Cube, RC, and G components are categorized to the recrystallization texture, as shown in Figure 11.

At the beginning of the annealing process in Figure 11a, the initial fraction of the deformation texture ranges from 3% to 12%, while the fraction of the recrystallization texture lies below 13% in Figure 11b. It is noted that the deformation texture decreases, but the recrystallization texture increases with increasing recrystallization fraction, that is, the annealing time at a fixed temperature. In the case of the recrystallization texture, the volume fractions of RC and G are below 10%, and these initial fractions are close to zero. However, the initial fraction of the Cube is about 12%, which suggests the Cube is retained during the hot-rolling process.

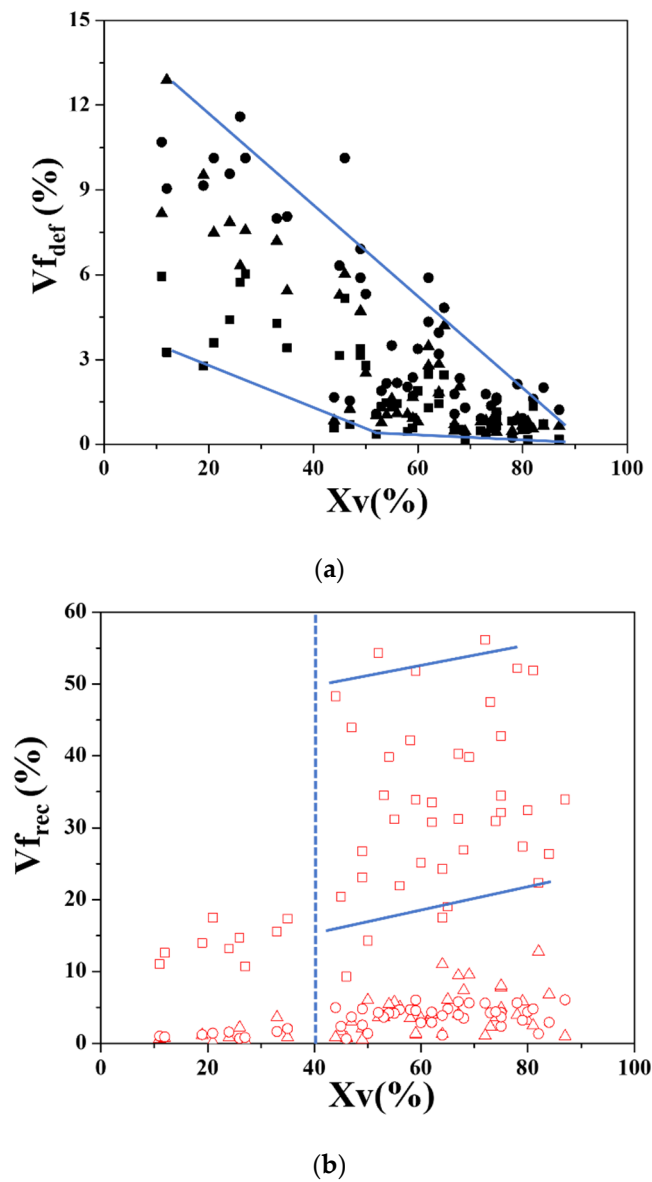


Figure 11. Volume fraction V_f of (a) deformation and (b) recrystallization components as a function of recrystallization fraction X_v for hot-rolled AA1100 alloy. (■: C, ●: S, ▲: B, □: Cube, ○: RC, △: G).

In order to investigate the effects of the 12 hot-rolling processing, we plot the volume fraction in terms of the recrystallization fraction for the six components of C, S, B, Cube, RC, and G, as shown in Figure 12. Firstly, considering the deformation texture of C, S, and B components, it is observed that the initial fraction of B, S, and C is 13%, 9%, and 3%, respectively, as in Figure 12a–c. By increasing the recrystallization fraction, the components of B and S decrease significantly more than the C component.

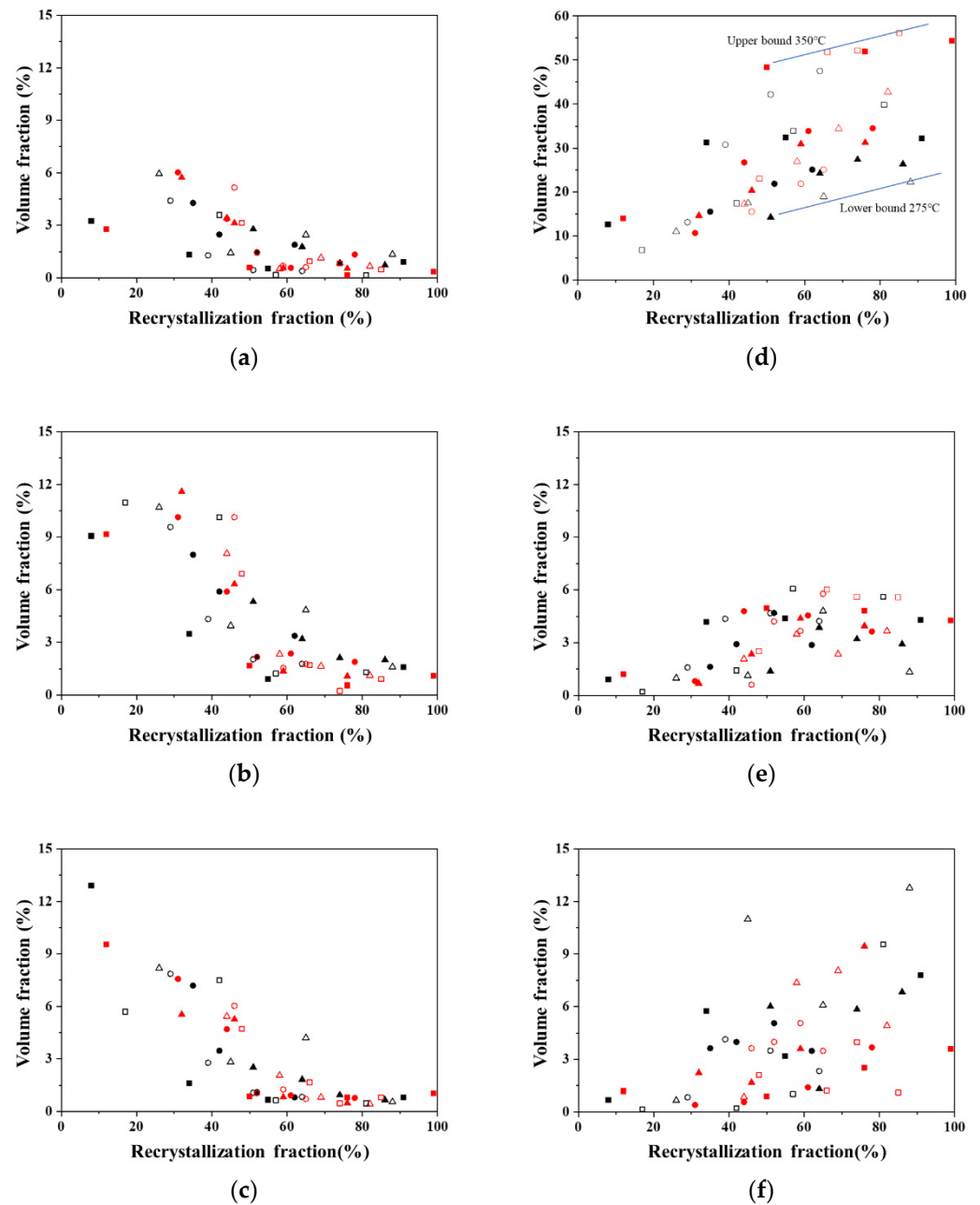


Figure 12. Volume fraction of (a) C, (b) S, (c) B, (d) Cube, (e) RC, and (f) G components as a function of annealing time at annealing temperatures of 275, 300, and 350 °C for hot-rolled AA1100 alloy. (▲ △: 275 °C, ● ○: 300 °C, ■ □: 350 °C; △ ○ □: 5/s, ▲ ● ■: 90/s).

For the recrystallization texture of Cube, RC, and G, the volume fractions of Cube and G are enhanced with the increasing recrystallization time in Figure 12d,f, while the RC component does not show a significant change in the volume fraction in Figure 12e. Furthermore, the Cube component plays an important role in the annealing process because the 50% fraction of Cube is larger than the 12% fraction of Goss. Thus, we take the Cube component into account for the following discussions between the 12 hot-rolling processing conditions and the texture components.

The 12 hot-rolling processing conditions in Table 4 present the various Z value defined by Equation (3). The smallest Z value was found for the strain rate of 5/s and the temperature of 350 °C, and the largest Z value was found for the strain rate of 90/s and the temperature of 275 °C. By increasing the strain rate and decreasing the temperature,

the Z value is enhanced. Figure 13 shows the volume fraction of the Cube component with respect to the recrystallization fraction for the 12 hot-rolling processing conditions. In comparison with the strain rate of 90/s in Figure 13b, the fraction of Cube is larger than that at the strain rate of 5/s in Figure 13a, and it has a larger fraction at 350 °C than at 275 °C. The conditions of 5/s and 350 °C correspond to the smallest Z value. It was also reported that the stability of the Cube orientation increases with the decreasing Z value [7,9,23].

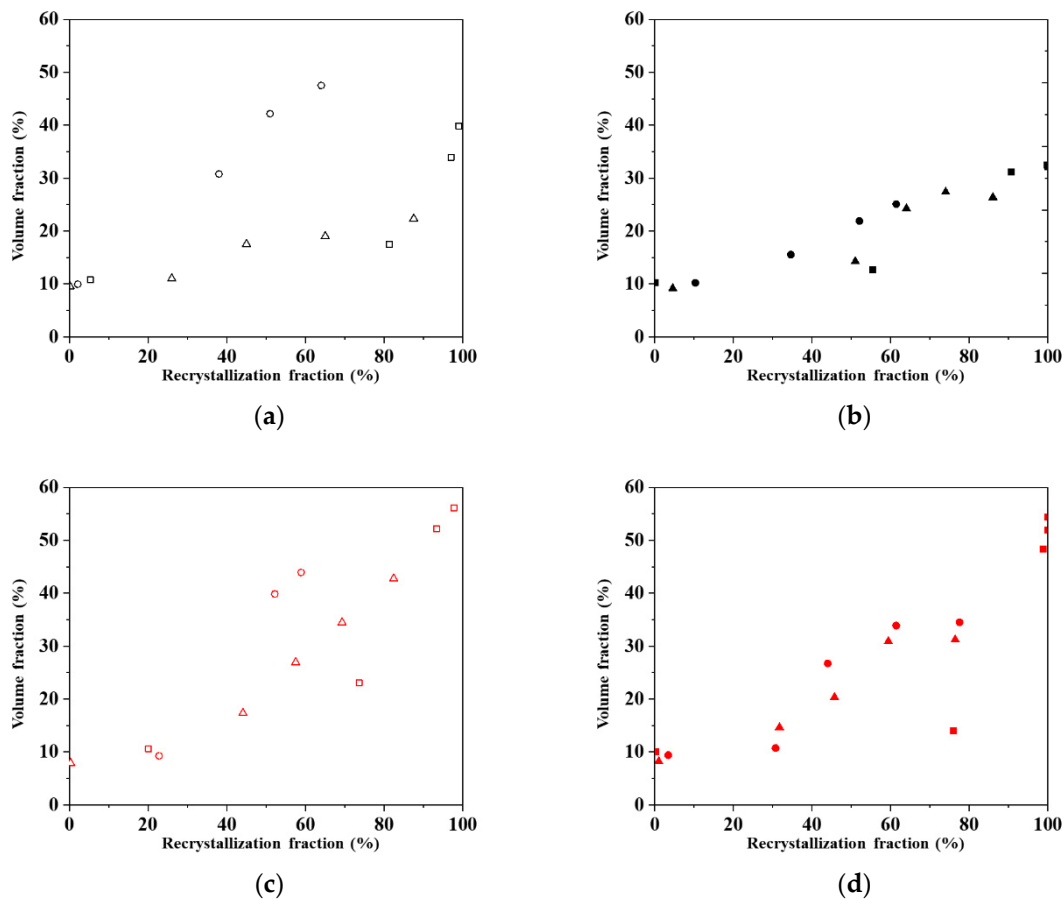


Figure 13. Volume fraction of Cube component at strain rates of (a,c) 5 s^{-1} and (b,d) 90 s^{-1} after (a,b) 60% and (c,d) 85% in hot-rolled AA1100 alloy. (▲, 275 °C; 90/s; ●, 300 °C; 90/s; ■, 350 °C; 90/s, △, 275 °C, 5/s; ○, 300 °C; 5/s, □, 350 °C, 5/s).

After the hot-rolled state before annealing, the 13% volume fraction of the Brass component is larger than the S and Copper components in Figure 12a–c. As increasing the recrystallized fraction, the β -fiber components decrease. The hot-rolled state before annealing already reveals a 10% recrystallization, in which the recrystallization texture component is dominated by the Cube component with a 10% volume fraction in Figure 12d. The Cube fraction increases markable in the range between 20% and 55% depending on the thermomechanical process conditions above 40% recrystallization. The presence of the $\{001\}\langle 100 \rangle$ orientation in the hot bands or shear bands of the deformation matrix resulted in the development of the Cube-dominating recrystallization texture [31–34]. The severe thickness reductions involved (above 98%) elevated temperatures and large inter-pass times between two consecutive rolling passes may induce static recrystallization in the breakdown rolling and lead to the evolution of Cube orientation [35]. Sidor et al. [36] claimed that the hot-rolling texture is composed of β -fibre and recrystallization texture of very weak Cube and Goss components at low finishing temperature ($T < 240 \text{ °C}$). At low roll finishing temperatures ($T \sim 250 \text{ °C}$), the formation of recrystallization texture components could be attributed to the enhanced interpass time by triggering the recrystallization process, which leads to β -fibers mixed with recrystallization components. Purely RX texture components

were observed at the increasing roll finishing temperatures ($T > 300\text{ }^{\circ}\text{C}$) [37]. The boundary relation between the recrystallization nuclei and a deformed matrix in Al has the rotation axis of the $\langle 772 \rangle$ axis with a rotation angle of $52\text{--}70^{\circ}$ [38].

Then, after annealing, the maximum volume fraction of the Cube component is 55% under the reduction of 85% with the strain rate of 5/s or 90/s at a high temperature of $350\text{ }^{\circ}\text{C}$ for complete recrystallization. However, it is about 50% under the reduction of 60% with the strain rate of 5/s at $300\text{ }^{\circ}\text{C}$, which shows 60% recrystallization. Kraner et al. [39] also reported that the 6 mm finished thickness of the hot-rolled band had 64% of the random texture components and 83% recrystallized grains, whereas the 3.25 mm thickness had 42% random texture components and 55% recrystallized grains. During the high-temperature and high-dwell-time annealing operation of the Al5052 sheet processed through high amounts of thickness reductions, Wu et al. [40] found that some grains take part in the static recrystallization mechanism, leading to grain refinement.

4. Conclusions

In this work, we tried to understand the effects of hot-rolling process conditions on the development of the recrystallization texture during the following annealing. Comparing the hot-rolling process conditions without annealing, it is noted that the 13% volume fraction of the Brass component is larger than the S and Copper components. The hot-rolled state shows the 10% volume fraction of the Cube component under the 10% recrystallization. Then, after annealing, the maximum fraction of the Cube component is 55% under the reduction of 85% with the strain rate of 5/s or 90/s at a high temperature of $350\text{ }^{\circ}\text{C}$ for complete recrystallization. The maximum fraction of the Cube is about 50% under the reduction of 60% with the strain rate of 5/s at $300\text{ }^{\circ}\text{C}$ for 60% recrystallization. This finding is of industrial importance in tailoring the texture components for different applications by varying the thermomechanical process conditions.

Author Contributions: Conceptualization, J.-C.K. and T.-Y.T.; methodology, C.-I.C.; software, S.-C.H.; validation, S.-C.H. and C.-I.C.; formal analysis, H.-L.Y.; investigation, H.-L.Y.; resources, T.-Y.T.; data curation, P.-J.C.; visualization, P.-J.C.; writing—review and editing, H.-L.Y.; supervision, J.-C.K.; project administration, J.-C.K.; funding acquisition, J.-C.K. All authors have read and agreed to the published version of the manuscript.

Funding: This research was funded by the National Science and Technology Council, grant number NSTC 112-2221-E-006-079. The authors gratefully acknowledge the use of EM000700 of Multi-function environmental field emission scanning electron microscope with EDS and EBSD belonging to the Core Facility Center of National Cheng Kung University.

Data Availability Statement: The data presented in this study are available on request from the corresponding author.

Conflicts of Interest: Chih-I Chang and Tien-Yu Tseng are employed by China Steel Corporation. The remaining authors declare that the research was conducted in the absence of any commercial or financial relationships that could be construed as a potential conflict of interest.

References

1. Jensen, D.J.; Hansen, N. Deformation and recrystallization textures in commercially pure aluminum. *Metall. Trans. A* **1986**, *17*, 253–259.
2. Hollinshead, P.A.; Sheppard, T. Development of Rolling Textures in Aluminum Alloy 3004 Subjected to Varying Hot-Rolling Deformation. *Metall. Trans. A* **1989**, *20*, 1495–1507. [[CrossRef](#)]
3. Bate, P.; Oscarsson, A. Deformation banding and texture in hot rolled Al-1.0Mn-1.2Mg alloy. *Mater. Sci. Technol.* **1990**, *6*, 520–527. [[CrossRef](#)]
4. Daaland, O.; Maurice, C.; Driver, J.; Raynaud, G.M.; Lequeu, P.; Strid, J.; Nes, E. Evolution of microstructure and texture during hot rolling and annealing of aluminium alloy 3004. In Proceedings of the 3rd International Conference on Aluminium Alloys Their Physical and Mechanical Properties (ICAA3), Trondheim, Norway, 22–26 June 1992.
5. Engler, O.; Wagner, P.; Ponge, D. Strain rate sensitivity of flow stress and its effect on hot rolling texture development. *Scr. Metall. Mater.* **1993**, *28*, 1317–1322. [[CrossRef](#)]

6. Panchanadeeswaran, S.; Field, D.P. Texture evolution during plane strain deformation of aluminum. *Acta Metall. Mater.* **1995**, *43*, 1683–1692. [[CrossRef](#)]
7. Vatne, H.E.; Shahani, R.; Nes, E. Deformation of cube-oriented grains and formation of recrystallized cube grains in a hot deformed commercial AlMgMn aluminium alloy. *Acta Mater.* **1996**, *44*, 4447–4462. [[CrossRef](#)]
8. Maurice, C.; Driver, J.H. Hot rolling textures of f.c.c. metals—Part I. Experimental results on Al single and polycrystals. *Acta Mater.* **1997**, *45*, 4627–4638. [[CrossRef](#)]
9. ADuckham, R.D.; Knutsen, O. Engler, Influence of deformation variables on the formation of copper-type shear bands in Al–1Mg. *Acta Mater.* **2001**, *49*, 2739–2749. [[CrossRef](#)]
10. Bate, P.S.; Huang, Y.; Humphreys, F.J. Development of the “brass” texture component during the hot deformation of Al–6Cu–0.4Zr. *Acta Mater.* **2004**, *52*, 4281–4289. [[CrossRef](#)]
11. Bacroix, B.; Brun, O.; Chauveau, T. The Influence of Temperature on the Rolling Textures of Al Alloys in the Absence of Recrystallization. *Textures Microstruct.* **1991**, *14–18*, 787–792. [[CrossRef](#)]
12. Samajdar, I.; Ratchev, P.; Verlinden, B.; Aernoudt, E. Hot working of AA1050-relating the microstructural and textural developments. *Acta Mater.* **2001**, *49*, 1759–1769. [[CrossRef](#)]
13. Aryshenskii, E.; Hirsch, J.; Konovalov, S.; Aryshenskii, V.; Drits, A. Influence of Mg Content on Texture Development during Hot Plain-Strain Deformation of Aluminum Alloys. *Metals* **2021**, *11*, 865. [[CrossRef](#)]
14. Le Hazif, R.; Dorizzi, D.; Poirier, J.P. Glissement {110}(110) dans les métaux de structure cubique faces centrées. *Acta Metall.* **1973**, *21*, 903–912. [[CrossRef](#)]
15. Le Hazif, R.; Poirier, J.P. Cross-slip on {110} planes in aluminum single crystals compressed along (100) axis. *Acta Metall.* **1975**, *23*, 865–871. [[CrossRef](#)]
16. Bacroix, B.; Jonas, J.J. The influence of non-octahedral slip on texture development in FCC metals. *Textures Microstruct.* **1988**, *8*, 267–311. [[CrossRef](#)]
17. Bacroix, B.; Jonas, J.J. *Proc. ICOTOM 8*; Kallend, J.S., Gottstein, G., Eds.; TMS: Warrendale, PA, USA, 1988.
18. Hirsch, J.; Luecke, K. Overview no. 76, Mechanism of deformation and development of rolling textures in polycrystalline f.c.c. metals—II. Simulation and interpretation of experiments on the basis of Taylor-type theories. *Acta Metall.* **1988**, *36*, 2883–2904. [[CrossRef](#)]
19. Maurice, C.L.; Driver, J.H.; Tóth, L.S. Modelling High Temperature Rolling Textures of FCC Metals. *Textures Microstruct.* **1992**, *19*, 211–227. [[CrossRef](#)]
20. Liu, W.C.; Morris, J.G. Effect of hot and cold deformation on the β fiber rolling texture in continuous cast AA 5052 aluminum alloy. *Scr. Mater.* **2005**, *52*, 1317–1321. [[CrossRef](#)]
21. Alvi, M.H.; Cheong, S.W.; Suni, J.P.; Weiland, H.; Rollett, A.D. Cube texture in hot-rolled aluminum alloy 1050 (AA1050)—Nucleation and growth behavior. *Acta Mater.* **2008**, *56*, 3098–3108. [[CrossRef](#)]
22. Wang, Y.; Yang, F.; Ren, L.; Liu, Q.; Cao, Y.; Huang, G. Microstructure and Texture of an Aluminum Plate Produced by Multipass Cold Rolling and Graded Annealing Process. *Metals* **2022**, *12*, 260. [[CrossRef](#)]
23. Crumbach, M.; Gottstein, G. Analysis of the activity of {110}<110> slip in AA3103 by inverse modeling. *Mater. Sci. Eng. A* **2004**, *387–389*, 282–287.
24. Maurice, C.; Driver, J.H. High temperature plane strain compression of cube oriented aluminium crystals. *Acta Metall. Mater.* **1993**, *41*, 1653–1664. [[CrossRef](#)]
25. Gatti, J.R.; Bhattacharjee, P.P. Effect of Prior Recovery Treatment on the Evolution of Cube Texture During Annealing of Severely Warm-Rolled Al-2.5 wt pctMg Alloy. *Metall. Mater. Trans. A* **2015**, *46*, 4966–4977. [[CrossRef](#)]
26. Sheppard, T.; Duan, X. Modelling of static recrystallisation by the combination of empirical models with the finite element method. *J. Mater. Sci.* **2003**, *38*, 1747–1754. [[CrossRef](#)]
27. Gutierrez, I.; Castro, F.R.; Urcola, J.J.; Fuentes, M. Static recrystallization kinetics of commercial purity aluminium after hot deformation within the steady state regime. *Mater. Sci. Eng. A* **1988**, *102*, 77–84. [[CrossRef](#)]
28. Sellars, C.M.; McTegart, W.J. On the mechanism of hot deformation. *Acta Metall.* **1966**, *14*, 1136–1138. [[CrossRef](#)]
29. McQueen, H.J.; Ryan, N.D. Constitutive analysis in hot working. *Mater. Sci. Eng. A* **2002**, *322*, 43–63. [[CrossRef](#)]
30. Wells, M.A.; Samarasekera, I.V.; Brimacombe, J.K.; Hawbolt, E.B.; Lloyd, D.J. Modeling the microstructural changes during hot tandem rolling of AA5XXX aluminum alloys: Part I. Microstructural evolution. *Metall. Mater. Trans. B* **1998**, *29*, 611–620. [[CrossRef](#)]
31. Sidor, J.J. Effect of Hot Band on Texture Evolution and Plastic Anisotropy in Aluminium Alloys. *Metals* **2021**, *11*, 1310. [[CrossRef](#)]
32. Cantergiani, E.; Riedel, M.; Karhausen, K.F.; Roters, F.; Quadfasel, A.; Falkinger, G.; Engler, O.; Rabindran, R. Simulations of Texture Evolution in the Near-Surface Region During Aluminum Rolling. *Metall. Mater. Trans. A* **2024**, *55*, 3327–3350. [[CrossRef](#)]
33. Cantergiani, E.; Weißensteiner, I.; Grasserbauer, J.; Falkinger, G.; Pogatscher, S.; Roters, F. Influence of Hot Band Annealing on Cold-Rolled Microstructure and Recrystallization in AA 6016. *Metall. Mater. Trans. A* **2023**, *54*, 75–96. [[CrossRef](#)]
34. Cho, J.-H.; Lee, G.-Y.; Lee, S.-H. Dynamic Shear Texture Evolution during the Symmetric and Differential Speed Rolling of Al-Si-Mg Alloys Fabricated by Twin Roll Casting. *Materials* **2024**, *17*, 179. [[CrossRef](#)]
35. Engler, O. Modelling of Microstructure and Texture and the Resulting Properties during the Thermo-Mechanical Processing of Aluminium Sheets. *Mater. Sci. Forum.* **2006**, *519–521*, 1563–1568. [[CrossRef](#)]

36. Sidor, J.J.; Petrov, R.H.; Kestens, L.A.I. Texture Control in Aluminum Sheets by Conventional and Asymmetric Rolling. In *Comprehensive Materials Processing*; Button, S.T., Ed.; Elsevier: Amsterdam, The Netherlands, 2014; Volume 3, pp. 447–498.
37. Hirsch, J. Texture Evolution and Earing in Aluminium Can Sheet. *Mater. Sci. Forum.* **2005**, *495–497*, 1565–1572.
38. Lobanov, M.L.; Zorina, M.A.; Reznik, P.L.; Redikultsev, A.A.; Pastukhov, V.I.; Karabanalov, M.S. Crystallography of Recrystallization in Al and Cu with Fiber Texture. *Metals* **2023**, *13*, 1639. [[CrossRef](#)]
39. Kraner, J.; Cvahte, P.; Šuštarč, P.; Šuštar, T.; Donik, Č.; Paulin, I.; Kim, S.K.; Kim, K.I. Effects of Variated Final Temperature and Workpiece Thickness for Hot Rolling of Aluminum Alloy EN AW-8011. *Metals* **2023**, *13*, 1301. [[CrossRef](#)]
40. Wu, J.; Djavanroodi, F.; Gode, G.; Ebrahimi, M.; Attarilar, S. Microstructure evolution, texture development, and mechanical properties of hot-rolled 5052 aluminum alloy followed by annealing. *Mater. Res. Express* **2022**, *9*, 056516. [[CrossRef](#)]

Disclaimer/Publisher’s Note: The statements, opinions and data contained in all publications are solely those of the individual author(s) and contributor(s) and not of MDPI and/or the editor(s). MDPI and/or the editor(s) disclaim responsibility for any injury to people or property resulting from any ideas, methods, instructions or products referred to in the content.